THE JOURNAL OF PHYSICAL CHEMISTRY Letters

Letter

pubs.acs.org/JPCL

Unravelling the Role of the Compressed Gas on Melting Point of Liquid Confined in Nanospace

Shimou Chen,[†,‡] Yusheng Liu,[†] Haiying Fu,[†] Yaxing He,[†] Cheng Li,[†] Wei Huang,[†] Zheng Jiang,[†] and Guozhong Wu*[,†]

[†]Shanghai Institute of Applied Physics, Chinese Academy of Sciences, Shanghai 201800, China

[‡]Institute of Process Engineering, Chinese Academy of Sciences, Beijing 100190, China.

Supporting Information

ABSTRACT: Phase behaviors of the liquids in nanospaces are of particular interest to understand the thermodynamics of the liquid on the nanoscale and for their applications that involve the confined systems. However, in many cases, the inconsistent observations of melting point variation for confined liquids are often revealed by different groups. Ionic liquids are a special kind of liquid. Here, by using the merits of the nonvolatile nature of ionic liquids, we realized the encapsulation of ionic liquids inside of mesopores silica oxide nanoparticles with a complete removal of compressed gas under high-vacuum condition; the completely confined ionic liquid formed a crystalline-like phase. It was found that compressed gas plays an important role in changing the melting point of the confined ionic liquid.

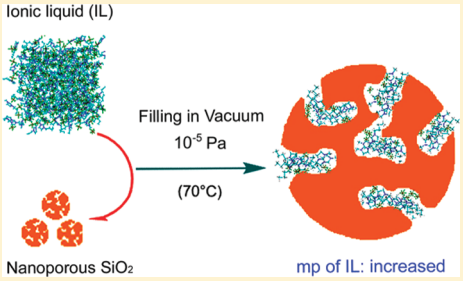

SECTION: Surfaces, Interfaces, Porous Materials, and Catalysis

The study of the behavior of liquid materials upon confinement is of great importance due to its relevance to microlubrication,[1] surface tribology,[2] retrieval and transport of liquids in rocks,[3] petroleum extraction,[4] molecular mobility in cells and membranes,[5] controlled drug release,[6] nanofluid-based nanodevices, and so forth. Most of the properties of a liquid are quite different from those of the bulk once it has been confined within a solid matrix. Many interesting phenomena have been reported concerning the effects of nanoconfinement on the change in melting point,[7] crystal structure,[8] and the chemical reactivity[9] of the confined species. For example, the melting point of water confined in nanopores can either be reduced or elevated depending upon the interfacial free energy, surface roughness, and contact angle.[10−12] Up to now, many of the predictions and arguments surrounding the variation in melting point of confined liquids have come only from theoretical calculations. This is due to inherent experimental difficulties in the preparation of complete nanoconfinement materials and in the probing of the properties of confined liquids.[13] Further experimental explorations are expected to provide greater insight into which factors predominantly determine the phase behavior of confined liquids. Due to the volatility of liquids, confined liquids always coexist with gases (including the compressed air originally existing in the nanocavities and the volatiles from the confined liquid) in nanospace,[14] leading to a more complicated system in which to determine the behavior of a confined liquid.

Room-temperature ionic liquids (ILs) are a special class of liquids solely composed of cations and anions. ILs are usually liquid at room temperature but have an extremely low vapor pressure. Therefore, they provide a good model liquid for handling in high vacuum. This is very important for the preparation of the genuine confined liquid by filling them into a nanospace; as the filling process can be done under vacuum condition, the final obtained confined liquids in composites are free from compressed gases and other volatiles. Furthermore, on the basis of the reported pioneering results, the spatially confined ILs in IL/inorganic hybrids have many appealing characteristics, such as excellent catalytic activities, high ionic conductivities, high heat resistance, and good tribological performance.[15−18] Studies on the phase behavior of confined ILs are of paramount importance from both the scientific and application points of view.

In conjunction with our ongoing efforts to investigate the phase behavior of ILs on the surface of mica,[19] graphite,[20] and silica nanoparticles[21] and inside of multiwalled carbon nanotubes,[22] in this study, we have sought a simple means by which to encapsulate ILs so that they are completely confined in the cavities of porous nanoparticles. Complete nanoconfinement of ILs was realized by heating a mixture of IL and mesoporous silica oxide particles (hereafter referred to as SiO_2) at high temperature under high vacuum. We found that the complete filling and close packing of the IL act as the dominant factors in the elevation of the melting point of the confined ILs. In contrast, when the IL is immobilized onto the surface of SiO_2 by filling at atmospheric pressure, the melting point of the IL is decreased in comparison with that of the bulk (Scheme 1).

Received: February 24, 2012
Accepted: April 5, 2012
Published: April 5, 2012

Scheme 1. Schematic Diagram of the Change in Melting Point of an IL Entrapped by Mesoporous Silica Oxide Particles under Vacuum Conditions versus that at Atmospheric Pressure

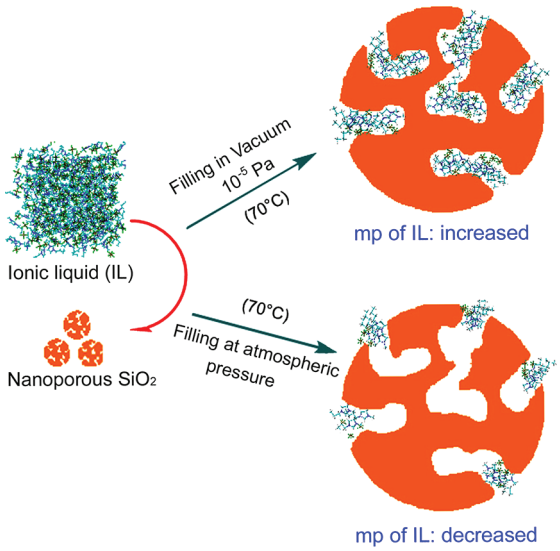

To elucidate the role and influence of the confinement effect on the melting point of the confined ILs, a widely studied IL, [BMIM][PF_6] (BMIM: 1-butyl-3-methyl-imidazolium), they were filled into mesoporous SiO_2 at 70 °C under conditions of ultrahigh vacuum (1×10^{-5} Pa; the experimental details are in the Supporting Information). The as-obtained IL-filled materials will heretofore be referred to as [BMIM][PF_6]@SiO_2. For comparison, a similar procedure was applied to the filling of [BMIM][PF_6] into SiO_2 at atmospheric pressure (exposed to air), in which the [BMIM][PF_6] and SiO_2 mixture was heated at 70 °C under normal pressure (in this case, the IL was immobilized on the surface of nanoparticles or the entrances of mesopores, which was confirmed by our microscopy observation). The final sample was named [BMIM][PF_6]/SiO_2 for simplicity. As for the sample obtained from filling under high vacuum, the compressed air present in the cavities of the SiO_2 was completely removed by evacuation, as proven by our nitrogen sorption (BET) measurement. The BET experiments were performed on SiO_2, [BMIM][PF_6]@SiO_2, and [BMIM][PF_6]/SiO_2, whose corresponding surface areas were 667, 10, and 55 m^2/g, respectively. The surface area of the porous SiO_2 nanoparticles was dramatically reduced after immobilizing the [BMIM][PF_6] at atmospheric pressure and almost vanished after filling with the IL under vacuum. This indicates that all of the cavities of the SiO_2 were filled by the [BMIM][PF_6] when the filling was conducted under high vacuum.

The phase behavior of the ILs obtained by the two different filling procudures was investigated by differential scanning calorimetry (DSC) analysis. As shown in Figure 1A, a clear difference in the melting point of the confined [BMIM][PF_6] was observed between filling under vacuum and that at atmospheric pressure. Filling under vacuum leads to an increase in the melting point up to 201.6 °C (Figure 1A-a), indicating the transformation of the IL to a high-melting-point solid phase upon nanoconfinement. This observation is similar to the filling of the same IL inside of multiwalled carbon nanotubes.[16] On the contrary, immobilization under normal pressure leads to a decrease of the melting point, as depicted in Figure 1A-b. The

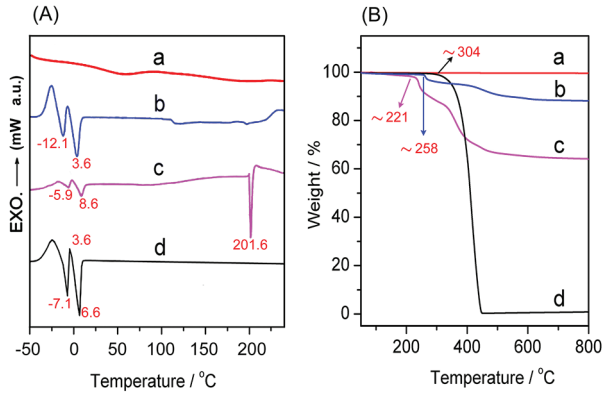

Figure 1. (A) DSC traces of mesoporous SiO_2 (a), [BMIM][PF_6]/SiO_2 (b), [BMIM][PF_6]@SiO_2 (c), and pure [BMIM][PF_6] (d). (B) TGA curves of mesoporous SiO_2 (a), [BMIM][PF_6]/SiO_2 (b), [BMIM][PF_6]@SiO_2 (c), and pure [BMIM][PF_6] (d).

DSC thermogram of the [BMIM][PF_6]/SiO_2 shows two peaks at 3.6 and −12.1 °C, lower than those of the pure [BMIM][PF_6] in bulk (Figure 1A-c). The DSC measurements were repeated many times, and the temperature variations were within ±0.5 °C for both of the samples; the opposite dependence of the melting point of [BMIM][PF_6] immobilized on the mesoporous SiO_2 via two different methods was reproduced. We suppose the packing states of the [BMIM]-[PF_6] in these two kinds of hybrids should be much different; for the [BMIM][PF_6]@SiO_2 sample, the main phase is a closely packed crystalline-like phase, and for the [BMIM][PF_6]/SiO_2, the amorphous state of the IL is the main form. This is further confirmed by our TEM and XRD measurements (see below).

Figure 1B shows the thermal gravity analysis (TGA) of mesoporous SiO_2, [BMIM][PF_6]@SiO_2, [BMIM][PF_6]/SiO_2, and the pure [BMIM][PF_6] in bulk. Two main weight-loss regions are found in the two kinds of hybrids (Figure 2B-b and c); the first step of the decomposition could be contributed to the breaking of end group alkyl chains of the [BMIM] ring, and the weight reduction in the second region is likely due to the total decomposition of the IL.[23] On the basis of the data of TGA, the loading amounts of the IL in [BMIM][PF_6]@SiO_2 and [BMIM][PF_6]/SiO_2 are 35.9 and 12.1 wt %, respectively. It should be mentioned that the onset of the confined IL in the [BMIM][PF_6]@SiO_2 sample is about 221 °C, which is much higher than the melting point value observed by DSC for the same sample, which proved that the observed thermal effects in DSC are not associated with some kind of thermal decomposition.

To further confirm that the increase of the melting point of nanoconfined ILs is a general phenomenon, two other ILs, [PMIM][PF_6] (PMIM: 1-propyl-3-methyl-imidazolium) and [AMIM][I] (AMIM: 1-allyl-3-methyl-imidazolium), were also confined in SiO_2 mesopores in a similar manner. As shown in Figure S1 (see Supporting Information), there is a considerable increase in the melting points of both [PMIM][PF_6]@SiO_2 and [AMIM][I]@SiO_2, in keeping with the results for nano-confined [BMIM][PF_6].

Transmission electron microscopy (TEM) was used to characterize the confined IL in mesoporous SiO_2. The iodine-containing IL [AMIM][I] was chosen in order to achieve a high resolution and contrast for TEM imaging. There was no significant difference in the TEM image of the mesoporous SiO_2, [AMIM][I]/SiO_2, and [AMIM][I]@SiO_2 by using the

dx.doi.org/10.1021/jz300225n | J. Phys. Chem. Lett. 2012, 3, 1052−1055

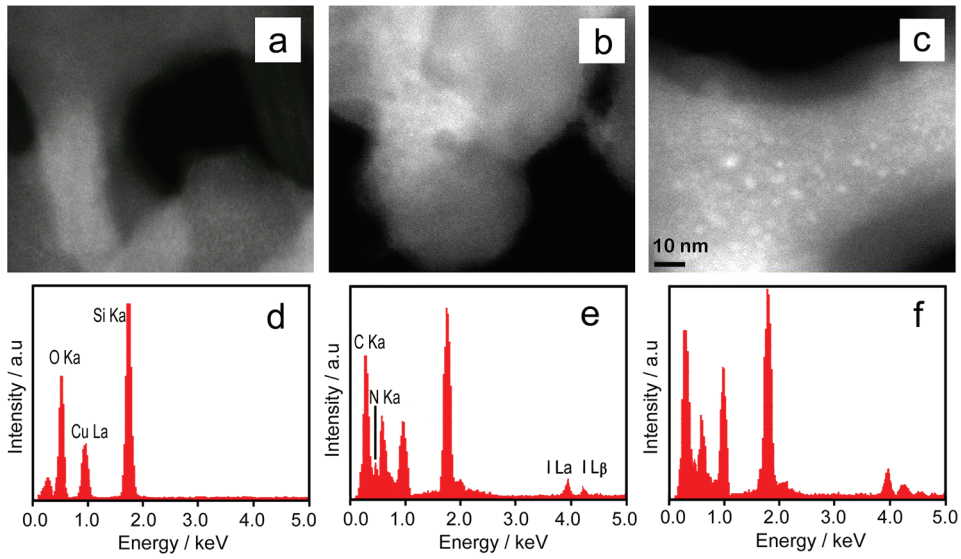

Figure 2. HAADF-STEM images and the corresponding EDX spectra of mesoporous SiO_2 (a, d), [AMIM][I]/SiO_2 (b, e), and [AMIM][I]@SiO_2 (c, f). The scale bare in (c) applies to all three images.

conventional TEM mode (see Supporting Information, Figure S2). The main cause is that the matrix SiO_2 is amorphous, which conceals the image contrasts of the samples. Fortunately, the IL in the nanocomposites can be discerned in the atomic-resolution high-angle annular dark-field (HAADF) images by scanning electron probe STEM mode due to the existence of heavy-atom iodine in [AMIM][I]. As shown in Figure 2, the confined IL in the [AMIM][I]@SiO_2 sample reveals clearly that some IL is encapsulated in the channel of SiO_2 (indicated by the white spots in Figure 3c). Even though the energy-dispersive X-ray (EDX) spectra confirmed that the [AMIM][I] ILs are present in both [AMIM][I]/SiO_2 and [AMIM][I]@SiO_2 (Figure 3e and f), extensive examination of HAADF images reveals that the white spots are only present in the [AMIM][I]@SiO_2 sample, indicating that the molecular packings of the [AMIM][I] in the two samples are much different. The confined IL obtained by conducting the filling process under high-vacuum condition (ie, [AMIM][I]@SiO_2 sample) shows strong signals of the heavy atom of iodine, which should be due to the formation of a crystalline-like phase of the IL in the completely confined space.[24] For the [AMIM][I]/SiO_2 sample, the immobilized IL may be mainly loosely dispersed on the surface of the SiO_2. In addition, the size of the white spots in [AMIM][I]@SiO_2 ranges from 2 to 5 nm, which is similar to the pore size of the SiO_2, and the white spots can be always observed by changing the focus of the electron beam (or depth sectioning), indicating that crystalline-like phases of the IL are inside of the mesoporous SiO_2, not adsorbed on the surface.[24]

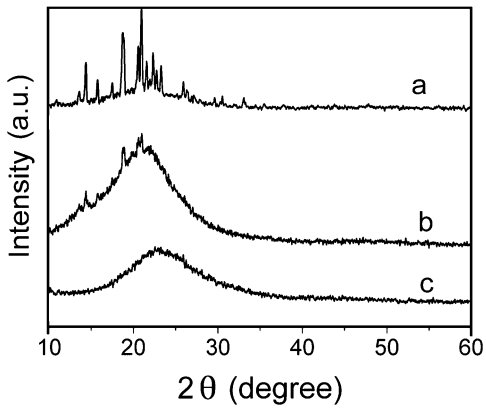

Figure 3. XRD pattern of [PMIM][PF_6]@SiO_2 (a), [BMIM][PF_6]@SiO_2 (b), and mesoporous SiO_2 (c).

The data of XRD further support the formation of the crystalline state of the confined ILs. Compared with the mesoporous SiO_2, some new peaks appeared at 2θ = 13.6, 15.9, 17.6, 20.0, and 20.8° for the sample of [PMIM][PF_6]@SiO_2 (Figure 3a); the new peaks should have originated from the confined [PMIM][PF_6]. The XRD pattern for [BMIM][PF_6]@SiO_2 shows clear peaks at 2θ = 13.8, 14.3, 18.6, and 20.8° (Figure 3b). These peaks have also been observed for [BMIM][PF_6] confined in a carbon nanotube or crystallized at −80 °C in the bulk (see Supporting Information, Figure S3), indicating that the [BMIM][PF_6] confined in the pores of the SiO_2 should exist in the form of a thermal stable crystal-like phase. Furthermore, the crystalline-like phases of the IL existing in the completely confined sample were further indicated by our Raman studies (the data and discussions are in the Supporting Information, Figure S4).

The phase transition behavior of the confined species can be explained with the use of simple mean field theory.[3] According to this theory, the melting point of a confined liquid (T_m) is given by

$$T_m = C(Z\varepsilon/k)$$

where C is a constant, Z is the number of nearest liquid neighbors, ε is interaction energy, and k is the Boltzmann constant. For instance, the interaction between [BMIM][PF_6] and the pore walls should be similar for both the [BMIM][PF_6]@SiO_2 and [BMIM][PF_6]/SiO_2 samples. The opposite sign of the change in melting point is thus attributed to the much greater number of nearest neighbors Z in [BMIM][PF_6]@SiO_2 than in [BMIM][PF_6]/SiO_2. Because we conducted the filling experiment under ultrahigh vacuum, which can remove all of the compressed gas from the cavities of the porous SiO_2, this ensured a close packing of the confined [BMIM][PF_6], leading

dx.doi.org/10.1021/jz300225n | J. Phys. Chem. Lett. 2012, 3, 1052−1055

to a greatly increased Z value. Furthermore, we suggest that in most of the literature, the liquid molecules were partly confined in the nanopores together with air because the filling process cannot be conducted under vacuum, owing to the evaporation of liquid. The existence of compressed gas inside of the pores leads to a small value of Z, which in turn leads to a decrease in the melting point. Therefore, by exploiting the nonvolatility of the IL, we first prepared a completely pure confined liquid in porous SiO_2 nanoparticles, permitting a firm conclusion regarding the melting point of a confined liquid; nanoconfinement effects absolutely lead to elevation of the melting point, but if the liquid coexists with gas in the confined space, the compressed gas will influence the phase behavior of the liquid. In many cases, the compressed gas plays an important role in the change of the melting point of the confined liquid, and this effect should be taken into consideration. It should be mentioned that the mean field theory is often applied to the system, in which liquid−liquid interaction is dominating; in our case, the melting temperature of the confined ILs should be also affected by the IL−SiO_2 interface and the IL−gas interface. For a more precise estimate of the melting point, the contribution from the surface tension of different interfaces has to be considered.

In summary, by the use of the nonvolatile property of ILs, we first realized encapsulation of ILs inside of mesopores of SiO_2 nanoparticles with a complete removal of the compressed gas by loading at high vacuum. It was found that the compressed gas plays an important role in the packing and phase behavior of the confined ILs. Without compressed gas, the nanoconfinement truly led to a considerable increase in the melting point of the confined ILs. These results are important for resolving many of the observed inconsistencies of the phase behavior of confined ILs and may stimulate more sophisticated studies on the low-dimensional physics and chemistry of liquids.

■ ASSOCIATED CONTENT

Supporting Information

Experimental details, characterizations, and Raman and XRD studies. This material is available free of charge via the Internet at http://pubs.acs.org.

■ AUTHOR INFORMATION

Corresponding Author

*E-mail: wuguozhong@sinap.ac.cn.

Notes

The authors declare no competing financial interest.

■ ACKNOWLEDGMENTS

This work was supported by the National Natural Science Foundation of China No. 11079007, 20973192, and 10705046.

■ REFERENCES

(1) Shimizu, I.; Martins, P. A. F.; Bay, N.; Andreasen, J. L.; Bech, J. I. Influences of Lubricant Pocket Geometry and Working Conditions upon Micro-lubrication Mechanisms in Upsetting and Strip Drawing. *Int. J. Surf. Sci. Eng.* **2010**, *4*, 42−54.

(2) Reiter, G.; Demirel, A. L.; Granick, S. From Static to Kinetic Friction in Confined Liquid Films. *Science* **1994**, *263*, 1741−1744.

(3) Gelb, L. D.; Gubbins, K. E.; Radhakrishnan, R.; Sliwinska-Bartkowiak, M. Phase Separation in Confined Systems. *Rep. Prog. Phys.* **1999**, *62*, 1573−1659.

(4) Devahastin, S.; Mujumdar, A. S. A Numerical Study of Mixing in a Novel Impinging Stream Inline Mixer. *Chem. Eng. J.* **2002**, *85*, 215−223.

(5) Xiu, P.; Zhou, B.; Qi, W. P.; Lu, H. J.; Tu, Y. S.; Fang, H. P. Manipulating Biomolecules with Aqueous Liquids Confined within Single-Walled Nanotubes. *J. Am. Chem. Soc.* **2009**, *131*, 2840−2845.

(6) Trofymluk, O.; Levchenko, A. A.; Navrotsky, A. Interfacial Effects on Vitrification of Confined Glass-Forming Liquids. *J. Chem. Phys.* **2005**, *123*, 194509.

(7) Alexiadis, A.; Kassinos, S. Molecular Simulation of Water in Carbon Nanotubes. *Chem. Rev.* **2008**, *108*, 5014−5034.

(8) Sloan, J.; Kirkland, A. I.; Hutchinson, J. L.; Green, M. L. H. Structural Characterization of Atomically Regulated Nanocrystals Formed within Single-Walled Carbon Nanotubes Using Electron Microscopy. *Acc. Chem. Res.* **2002**, *35*, 1054−1062.

(9) Koshino, M.; Niimi, Y.; Nakamura, E.; Kataura, H.; Okazaki, T.; Suenaga, K.; Iijima, S. Analysis of the Reactivity and Selectivity of Fullerene Dimerization Reactions at the Atomic Level. *Nat. Chem.* **2010**, *2*, 117−124.

(10) Koga, K.; Zeng, X. C.; Tanaka, H. Freezing of Confined Water: A Bilayer Ice Phase in Hydrophobic Nanopores. *Phys. Rev. Lett.* **1997**, *79*, 5262−5265.

(11) Takaiwa, D.; Hatano, I.; Koga, K.; Tanaka, H. Phase Diagram of Water in Carbon Nanotubes. *Proc. Natl. Acad. Sci. U.S.A.* **2008**, *105*, 39−43.

(12) Reategui, E.; Aksan, A. Effects of the Low-Temperature Transitions of Confined Water on the Structures of Isolated and Cytoplasmic Proteins. *J. Phys. Chem. B* **2009**, *113*, 13048−13060.

(13) Cicero, G.; Grossman, J. C.; Schwegler, E.; Gygi, F.; Galli, G. Water Confined in Nanotubes and between Graphene Sheets: A First Principle Study. *J. Am. Chem. Soc.* **2008**, *130*, 1871.

(14) Miachon, S.; Syakaev, V. V.; Rakhmatullin, A.; Pera-Titus, M.; Caldarelli, S.; Dalmon, J. A. Higher Gas Solubility in Nanoliquids? *ChemPhysChem* **2008**, *9*, 78−82.

(15) Wasserscheid, P.; Welton, T. *Ionic Liquids in Synthesis*; Wiley-VCH: Weinheim, Germany, 2008.

(16) Armand, M.; Endres, F.; MacFarlane, D. R.; Ohno, H.; Scrosati, B. Ionic-Liquid Materials for the Electrochemical Challenges of the Future. *Nat. Mater.* **2009**, *8*, 621−629.

(17) Baldelli, S. Surface Structure at the Ionic Liquid−Electrified Metal Interface. *Acc. Chem. Res.* **2008**, *41*, 421−431.

(18) Zhou, F.; Liang, Y. M.; Liu, W. M. Ionic Liquid Lubricants: Designed Chemistry for Engineering Applications. *Chem. Soc. Rev.* **2009**, *38*, 2590−2599.

(19) Liu, Y.; Zhang, Y.; Wu, G.; Hu, J. Coexistence of Liquid and Solid Phases of Bmim-PF_6 Ionic Liquid on Mica Surfaces at Room Temperature. *J. Am. Chem. Soc.* **2006**, *128*, 7456−7457.

(20) Sha, M. L.; Zhang, F. C.; Wu, G. Z.; Fang, H. P.; Wang, C. L.; Chen, S. M.; Zhang, Y.; Hu, J. Ordering Layers of [bmim][PF6] Ionic Liquid on Graphite Surfaces: Molecular Dynamics Simulation. *J. Chem. Phys.* **2008**, *128*, 134504.

(21) Liu, Y. S.; Wu, G. Z.; Fu, H. Y.; Jiang, Z.; Chen, S. M.; Sha, M. L. Immobilization and Melting Point Depression of Imidazolium Ionic Liquids on the Surface of Nano-SiOx Particles. *Dalton Trans.* **2010**, *39*, 3190−3194.

(22) Chen, S. M.; Wu, G. Z.; Sha, M. L.; Huang, S. R. Transition of Ionic Liquid [bmim][PF6] from Liquid to High-Melting-Point Crystal When Confined in Multiwalled Carbon Nanotubes. *J. Am. Chem. Soc.* **2007**, *129*, 2416−2417.

(23) Singh, M. P.; Singh, R. K.; Chandra, S. Thermal Stability of Ionic Liquid in Confined Geometry. *J. Phys. D: Appl. Phys.* **2010**, *43*, 092001.

(24) Ortalan, V.; Uzun, A.; Gates, B. C.; Browning, N. D. Direct Imaging of Single Metal Atoms and Clusters in the Pores of Dealuminated HY Zeolite. *Nat. Nanotechnol.* **2010**, *5*, 506−510.